RADIO ASTRONOMY

A luminous fast radio burst that probes the Universe at redshift 1

S. D. Ryder[1,2], K. W. Bannister[3], S. Bhandari[4,5], A. T. Deller[6], R. D. Ekers[3,7], M. Glowacki[7], A. C. Gordon[8], K. Gourdji[6], C. W. James[7], C. D. Kilpatrick[8,9], W. Lu[10,11], L. Marnoch[1,2,3,12], V. A. Moss[3], J. X. Prochaska[13,14], H. Qiu[15], E. M. Sadler[3,16], S. Simha[13], M. W. Sammons[7], D. R. Scott[7], N. Tejos[17], R. M. Shannon[6]*

Fast radio bursts (FRBs) are millisecond-duration pulses of radio emission originating from extragalactic distances. Radio dispersion is imparted on each burst by intervening plasma, mostly located in the intergalactic medium. In this work, we observe the burst FRB 20220610A and localize it to a morphologically complex host galaxy system at redshift 1.016 ± 0.002. The burst redshift and dispersion measure are consistent with passage through a substantial column of plasma in the intergalactic medium and extend the relationship between those quantities measured at lower redshift. The burst shows evidence for passage through additional turbulent magnetized plasma, potentially associated with the host galaxy. We use the burst energy of 2×10^{42} erg to revise the empirical maximum energy of an FRB.

Fast radio bursts (FRBs) (*1*, *2*) are transient radio sources that last a few milliseconds, emitted by extragalactic sources. Free electrons along the path between the FRB source and Earth impart a frequency-dependent time delay (dispersion) on the radio signal. This dispersion can be used to measure the column density of free electrons [quantified by the dispersion measure (DM)] between the FRB source and the observer. FRBs localized to host galaxies at different redshifts exhibit a positive correlation between the extragalactic DM and host redshift, known as the Macquart relation (*3*). This relation has been used to measure the cosmic baryon fraction and the expansion rate of the Universe (*4*). This relation has been measured using identified FRB host galaxies at nearby redshifts of $z \lesssim 0.5$. Some unlocalized FRBs (with unknown host galaxies) have DMs consistent with $z > 1$ (*5*); however, an FRB associated with a galaxy at $z = 0.241$ had a high DM that would have implied $z > 1$ if its host had been unknown (*6*). This demonstrates that estimates of redshift from DM alone can be misleading if they are affected by plasma within the host galaxy—which also imparts a contribution to the DM—in addition to that of the intergalactic medium.

[1]School of Mathematical and Physical Sciences, Macquarie University, Sydney, NSW 2109, Australia. [2]Astrophysics and Space Technologies Research Centre, Macquarie University, Sydney, NSW 2109, Australia. [3]Australia Telescope National Facility, Commonwealth Science and Industrial Research Organisation, Space and Astronomy, Epping, NSW 1710, Australia. [4]Netherlands Institute for Radio Astronomy (ASTRON), 7991 PD Dwingeloo, Netherlands. [5]Joint institute for Very Long Baseline Interferometry in Europe, 7991 PD Dwingeloo, Netherlands. [6]Centre for Astrophysics and Supercomputing, Swinburne University of Technology, Hawthorn, VIC 3122, Australia. [7]International Centre for Radio Astronomy Research, Curtin Institute of Radio Astronomy, Curtin University, Perth, WA 6102, Australia. [8]Center for Interdisciplinary Exploration and Research in Astrophysics, Northwestern University, Evanston, IL 60208, USA. [9]Department of Physics and Astronomy, Northwestern University, Evanston, IL 60208, USA. [10]Department of Astronomy University of California, Berkeley, CA 94720, USA. [11]Theoretical Astrophysics Center, University of California, Berkeley, CA 94720, USA. [12]Australian Research Council Centre of Excellence for All Sky Astrophysics in 3 Dimensions (ASTRO 3D), Macquarie University, Sydney, NSW 2109, Australia. [13]Department of Astronomy and Astrophysics, University of California, Santa Cruz, CA 95064, USA. [14]Kavli Institute for the Physics and Mathematics of the Universe, Kashiwa, 277-8583, Japan. [15]Square Kilometre Array Observatory, Jodrell Bank, Lower Withington, Macclesfield SK11 9FT, UK. [16]Sydney Institute for Astronomy, School of Physics, University of Sydney, Sydney, NSW 2006, Australia. [17]Instituto de Física, Pontificia Universidad Católica de Valparaíso, Casilla 4059, Valparaíso, Chile.
*Corresponding author. Email: rshannon@swin.edu.au

Observations of FRB 20220610A

FRBs have been searched for (*7*) and localized (*8*) using the Australian Square Kilometre Array Pathfinder (ASKAP) (*9*), a radio interferometer in Western Australia comprising 36 antennas, each 12 m in diameter. Each antenna is equipped with a phased array receiving system, which provides 36 beams across the focal plane, covering ~30 square degrees. FRBs are searched for in real time using the incoherent sum of the intensities of each antenna in each beam. When an FRB is detected, temporary voltage buffers are downloaded, correlated, calibrated, and imaged; this enables the positions of detected bursts to be measured with an absolute precision of typically a few tenths of an arc second (*10*, *11*).

We detected FRB 20220610A in observations taken around the position of the previously known burst FRB 20220501C, but the two bursts are not related (*11*). The observations were centered at a frequency of 1271.5 MHz and had a time resolution of 1.18 ms. The dispersion of FRB 20220610A indicated a DM of $1458.15^{+0.25}_{-0.55}$ pc cm^{-3} (where pc is parsecs). This is higher than all but one of the 55 FRBs that were previously observed using ASKAP (*4*). A dedispersed dynamic spectrum of the burst is shown in Fig. 1, and observed properties of the burst are listed in Table 1. The burst does not show the 10- to 100-MHz modulation in

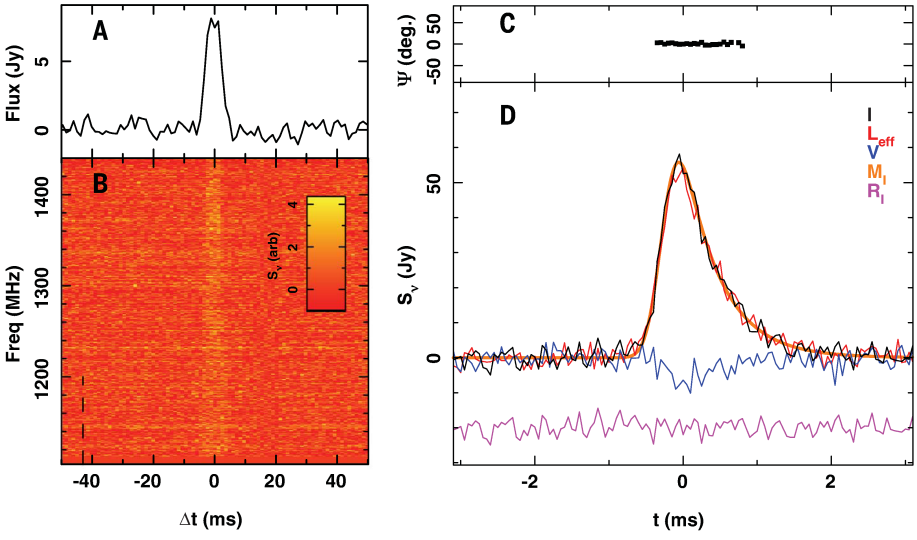

Fig. 1. Radio observations of FRB 20220610A. (**A** and **B**) The burst as observed in the incoherently summed data stream used by the real-time detection system. The pulse width is dominated by intrachannel dispersion smearing. (A) The integrated flux density (S_ν) of the pulse profile as a function of time (t). (B) The dedispersed burst dynamic spectrum as a function of frequency (Freq). The vertical dashed line in (B) indicates the frequency range (<1200 MHz) of high–time resolution data that were saved by the pipeline; data at higher frequencies were lost as a result of latency issues (see the text for details). (**C** and **D**) High–time resolution data (frequencies <1200 MHz) produced from the raw electromagnetic field samples saved from each telescope after the real-time trigger (*11*). (C) Linear polarization position angle Ψ during the pulse. (D) The integrated pulse profile in total intensity *I* (black), linear polarization $L_{\rm eff}$ (red), Stokes *V* (blue), and a maximum likelihood model of Stokes *I*, denoted M_I (orange). The residuals R_I (pink) between *I* and M_I are shown offset from zero by −20 Jy for clarity. The polarization position angle Ψ is defined such that linear polarization is in one Stokes parameter and hence Ψ ≈ 0.

the spectrum characteristic of many lower-DM, high–Galactic latitude ASKAP-detected FRBs (*7*).

The 2-s dispersive sweep of the burst across the instrument bandwidth and the 2.4-s latency in the detection system resulted in only the lowest 88 MHz of the burst being captured in the 3.1-s-duration voltage buffer. This was sufficient to localize the burst to a precision of 0.5 arc sec. We used the voltage data to reconstruct the high time resolution and polarimetric properties of the burst (*11*). After correcting for dispersive smearing, the burst shows an exponentially decreasing tail (Fig. 1D), which is consistent with scatter broadening as a result of turbulence in intervening plasma (*12*). We measure the pulse broadening time to be 0.511 ± 0.012 ms at a reference frequency of 1147.5 MHz, assuming a ν^{-4} frequency dependence (where ν is the frequency).

Ordered magnetic fields in astrophysical plasmas add additional, polarization-dependent dispersion. This manifests as wavelength-dependent variation in the linear polarization position angle, referred to as Faraday rotation (*13*). FRB 20220610A exhibits Faraday rotation, with a rotation measure (RM) of 215 ± 2 rad m^{-2}. After correcting for this Faraday rotation, we calculate that the burst had an intrinsic linear polarization fraction of 96 ± 1%. The high fractional linear polarization allows us to place a 67% upper limit on the Faraday dispersion (σ_{RM} < 0.6 rad m^{-2}) induced by fluctuations in the RM in intervening turbulent plasma. Higher levels of Faraday dispersion have been detected for other FRBs (*14*). The burst also shows lower fractional circular polarization of 10 ± 1%. Although instrumental artifacts can induce spurious circular polarization, we do not see any correlation between the Stokes polarization parameters *U* and *V* in the spectrum, which would be expected for an instrumental effect (*11*). The FRB was located ~4 arc min from the beam center, which makes off-axis leakage effects unlikely (*15*). Circular polarization has been observed in some FRBs and could either be intrinsic to the burst (*16*) or result from propagation through relativistic plasma in the immediate source environment (*17*).

Table 1. Properties of FRB 20220610A and its host galaxy. The fluence was derived from filter bank data that include the full ASKAP bandwidth. UTC, coordinated universal time; S/N, signal-to-noise ratio; FWHM, full width at half maximum. The host photometry is expressed in magnitudes (mag) on the AB system. The star formation rate (SFR) is in solar masses per year ($M_\odot$ year^{-1}). 100 Myr SFR is the integrated star formation in the past 100 million years (Myr). *Z*, metallicity of the host galaxy; $Z_\odot$, metallicity of the Sun.

Measured burst properties	
DM	$1458.15^{+0.25}_{-0.55}$ pc cm^{-3}
Topocentric arrival time at 1104 MHz (UTC)	2022-06-10 22:26:44.313
Fluence	45 ± 5 Jy ms
Right ascension (J2000 equinox)	23^{h}24^{m}17^s.569 ± 0^s.040
Declination (J2000 equinox)	−33°30′49″.37 ± 0″.50
Galactic longitude	8.83954°
Galactic latitude	−70.18569°
Incoherent detection S/N (1104–1440 MHz)	29.8
Image S/N (1104–1152 MHz)	81
RM	215 ± 2 rad m^{-2}
Inferred burst properties	
Intrinsic width (FWHM)	0.41 ± 0.01 ms
Implied FRB isotropic energy density	6 × 10^{32} erg Hz^{-1}
Milky Way disk DM contribution	31 pc cm^{-3}
Measured host galaxy properties	
Redshift	1.016 ± 0.002
Photometry:	
Band (central wavelength, Å)	Magnitude (mag)
g (4700)	24.15 ± 0.07
V (5510)	23.89 ± 0.13
R (6580)	23.78 ± 0.06
I (8060)	22.17 ± 0.07
z (9620)	21.95 ± 0.12
J (12,200)	21.97 ± 0.07
K_s (21,460)	22.08 ± 0.12
Inferred host galaxy properties	
Mass-weighted age	$1.02^{+1.64}_{-0.62}$ Gyr
log(stellar mass)	$9.98^{+0.14}_{-0.07}$ $M_\odot$
log(total mass)	$10.11^{+0.18}_{-0.07}$ $M_\odot$
100 Myr SFR	$0.42^{+0.83}_{-0.37}$ $M_\odot$ year^{-1}
log($Z/Z_\odot$)	$-0.11^{+0.17}_{-1.68}$

Host galaxy properties

We performed follow-up ground-based optical and infrared observations with the Very Large Telescope (VLT) and the W. M. Keck Observatory to identify and characterize the host galaxy of FRB 20220610A (*11*). The images (Fig. 2, A to C) show an object at the FRB location that has an extended, multicomponent morphology. We label the optical source that overlaps the radio position of the FRB as component (a) and two adjacent sources as components (b) and (c) (Fig. 2A). We use a Bayesian method to assess the chance of coincidence between a radio transient and optical galaxies (*18*), finding >99.99% confidence that the FRB is associated with component (a).

We performed broad-band optical and infrared spectroscopy of components (a), (b), and (c) (Fig. 2, D and E) (*11*). We identify two emission lines in the spectra as the [O II] 3726 and 3729 Å doublet, which is most prominent in the spectrum of component (b) (fig. S2). We measure the redshift of each component from this doublet, finding that they are all consistent with z = 1.016 ± 0.002.

We use the photometry and a stellar population model to estimate the total mass of the three components combined as 10^{10} solar masses, with a star formation rate of ~0.42 solar masses per year (*11*). These values, in addition to the estimated host metallicity and star formation history, are consistent with those of nearby FRB hosts (*19*, *20*), but the source morphology is markedly different. Observed and estimated properties of the host galaxy are also listed in Table 1.

The presence of two bright components (a) and (c) separated by 2.0 arc sec (which corresponds to a distance of 16 kpc at that redshift), and the diffuse feature (b) between them, is consistent with two galaxies interacting or merging or with a compact galaxy group. It is also possible that the morphology is due to

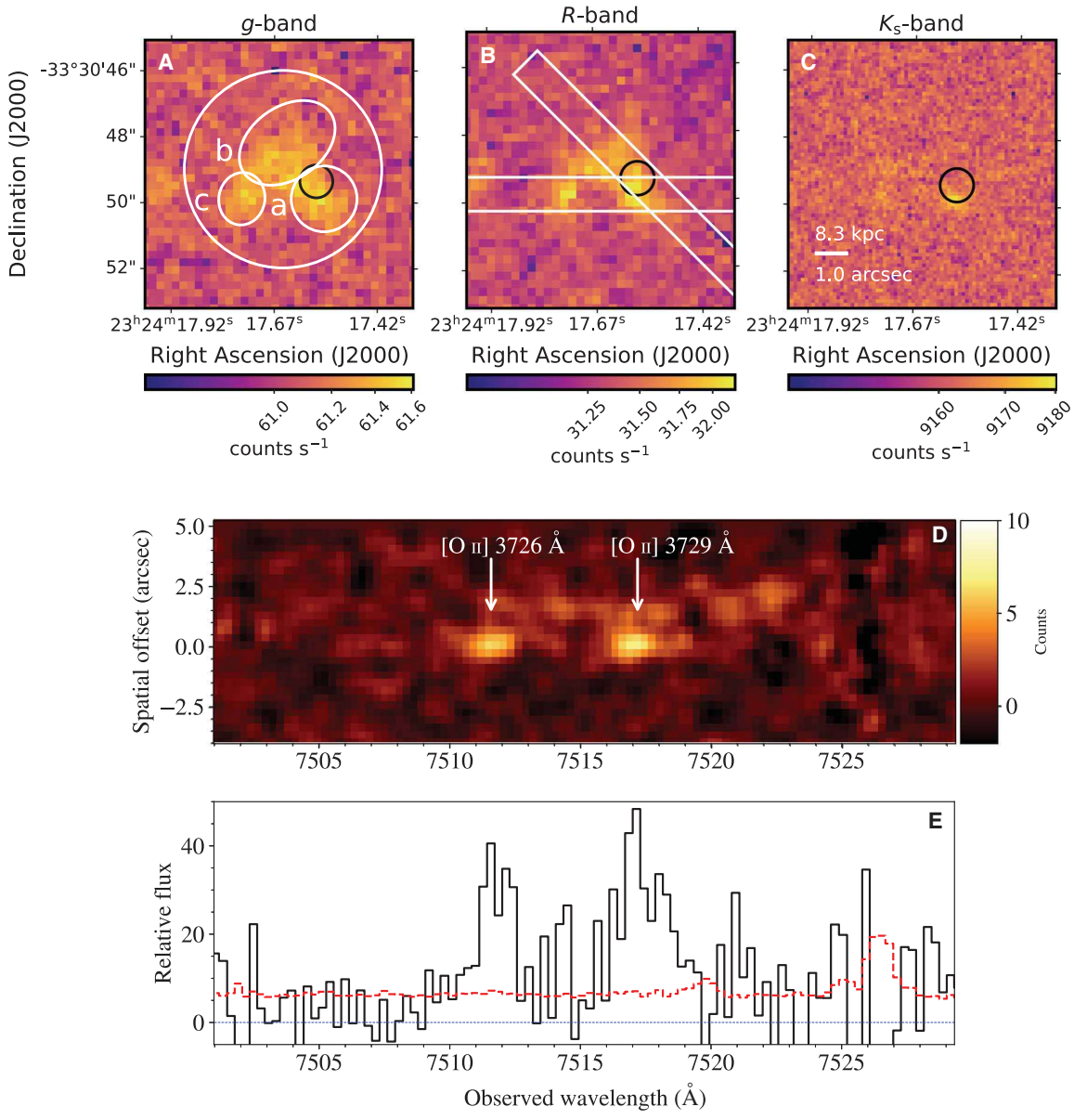

Fig. 2. Optical and infrared observations of the host galaxy of FRB 20220610A. In (A) to (C), the FRB localization and its uncertainty (68% confidence) are indicated by the black ellipse. (**A**) Optical *g*-band VLT image. White ellipses outline the apertures used for the photometry of each component (table S2). The larger unlabeled white circle is the aperture used for the entire combined system. (**B**) Optical *R*-band image. White rectangles outline the slit locations used for VLT spectroscopy. (**C**) Infrared K_S-band image. The scale bar applies to (A) to (C); it shows the angular scale and corresponding projected physical scale at the measured host redshift. The color bar below each panel indicates relative count rates in each processed image. (**D**) Two-dimensional (2D) VLT spectroscopy at a slit position angle on the sky of 45° covering components (a) and (b), as marked in (B). White arrows indicate two lines due to the [O II] doublet, with rest wavelengths of 3726 and 3729 Å. (**E**) 1D spectrum (black solid line) and its uncertainty (red dashed line) extracted from the 2D spectrum in (D), centered on the peak of the [O II] lines using an aperture width of 1.8″. The blue line indicates zero relative flux in arbitrary units.

internal structure within a single galaxy; at these redshifts, about half of all galaxies have clumpy morphologies (*21*). We regard the latter possibility as unlikely because of the large spatial separation between the components. Only component (a) is detected in the near-infrared (K_s-band) image (Fig. 2C), which indicates that it hosts an older stellar population compared with the other components. Component (a) is also displaced from the centroid of the total optical light in the *g*- and *R*-bands, contrary to what would be expected if it was the nuclear bulge of a single galaxy.

Extending the Macquart relation

We used the measured properties of FRB 20220610A to investigate the Macquart relation out to $z \sim 1$, by comparing the observed DM with predictions based on previous measurements of the relation at $z \leq 0.522$. Figure 3 shows the relationship between DM and redshift for the FRBs detected by ASKAP (*4*). We restrict our analysis to the ASKAP sample to reduce the effect of selection effects, which depend on the observing system. We do not refit the Macquart relation because doing so in an unbiased way would require a reanalysis of the entire updated FRB sample from ASKAP.

After subtracting a model Milky Way foreground contribution to the observed DM (*11*), we estimate the non-Galactic DM of FRB 20220610A to be ≈1376 pc cm^{-3}, indicating a high column density of ionized gas between the FRB and Earth. This is higher than the DM expected from the Macquart relation, by ~650 pc cm^{-3}, which is a 2.4σ excess (*11*). If the excess is real and originates from the host galaxy, the implied electron column density is 1300^{+170}_{-320} pc cm^{-3} in the host rest frame (*11*), with the uncertainty reflecting the intrinsic variation in the contribution from the intergalactic medium.

Interpretation of the DM

We use the scatter broadening and Faraday rotation of FRB 20220610A to investigate the properties of plasma at $z \approx 1$. A dispersion excess could potentially arise from any combination of gas in the immediate vicinity of the source, the interstellar medium of the host galaxy, or foreground gas along the line of sight—any of which could host turbulent

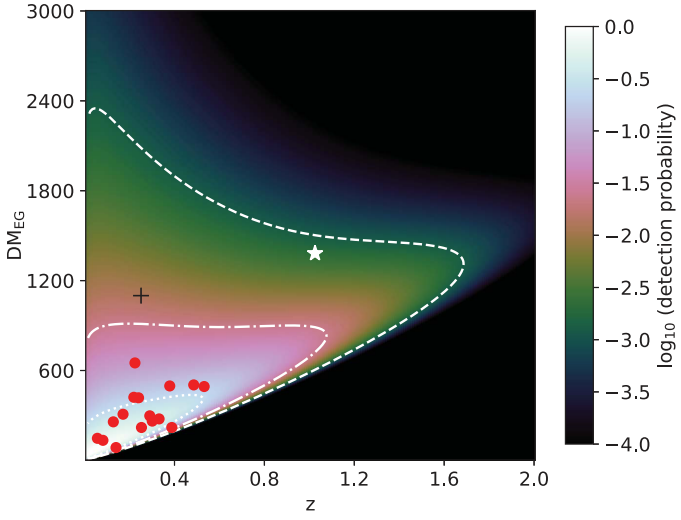

Fig. 3. Relationship between redshift and extragalactic DM for FRBs. Data are from the ASKAP incoherent sum survey (*4*). The extragalactic dispersion (DM_{EG}) is the contribution to DM after subtraction of a model for the Milky Way (*11*). Red circles indicate localized FRBs at the host galaxy redshifts. The color scale indicates an estimated detection probability, assuming a maximum energy density of $\log_{10}\left|\frac{E_\nu}{\text{erg Hz}^{-1}}\right| = 32.7 \pm 0.2$ (this work). White contours enclose 50% (dotted), 90% (dash-dot), and 99% (dashed) of the probability. The white star is FRB 20220610A. The black cross shows the repeating FRB 20190520B, which was excluded from the population inference because of differing selection effects between instruments (*28*). The uncertainties for all measurements are smaller than the symbol sizes.

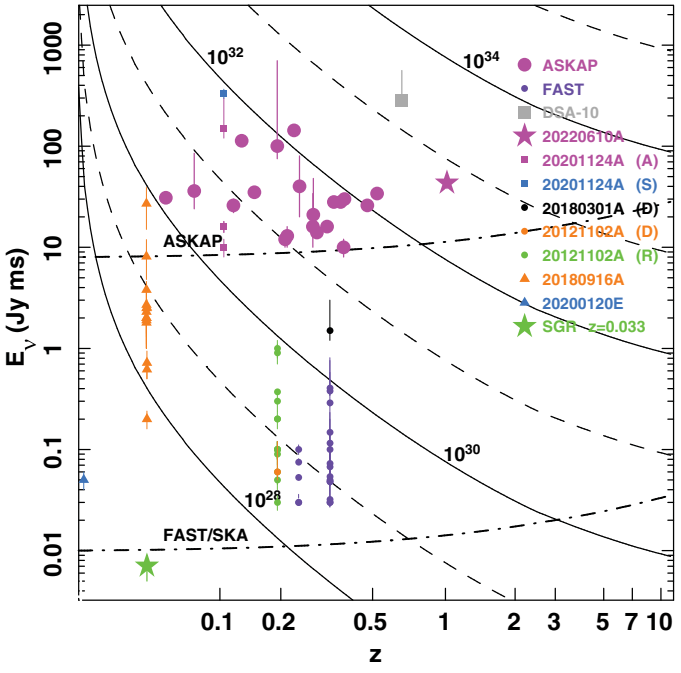

Fig. 4. Logarithmic plot of fluence as a function of redshift for localized FRBs. The magenta star is FRB 20220610A. Other notable FRBs are labeled using their Transient Name Server designations, omitting the FRB prefix for brevity. The curved solid and dashed contours indicate the energy density in units of ergs per hertz. The dash-dotted lines show the detection sensitivity of the ASKAP incoherent sum FRB search system, the Five-hundred-meter Aperture Spherical Telescope (FAST), and that expected for the Square Kilometre Array (SKA). Repeating FRBs are shown at multiple points at the same redshift but different fluences. Plotting symbols are indicated in the legend, which also indicates the FRB localization instruments. DSA, Deep Synoptic Array. The green star shows the expected fluence of the FRB-like burst from the Galactic magnetar SGR 1935+21 (*31*, *32*) if it were placed at the distance of the host galaxy of FRB 20180916A. There are biases in FRB searches that may result in the first detections of repeating sources having different properties than subsequent detections, particularly those made with other facilities (*33*). We therefore plot the repeating FRB 20201124A twice—for observations from ASKAP (designated A) (*17*) and the 25-m Stockert radio telescope (S) (*34*). For the repeating FRB 20121102A, we plot separately the initial detection (D) (*35*) and a sample of follow up bursts detected with a different instrument (R) (*36*). FRB 20180916A (*37*) and FRB 20200120E (*38*) are low-redshift repeating FRB sources. Other burst properties are reported from ASKAP (*3*, *4*, *8*, *27*), DSA-10 (*39*), and FAST observations of the repeating FRB 20180301A (*40*) and FRB 20190520D (*6*). For FRB 20180301A, we also plot the initial detection with a different instrument (D) (*41*).

magnetized plasma. For FRB 20220610A, there is an absence of strong ($\gtrsim 10^4$ rad m^{-2}) Faraday rotation or detectable depolarization; this is unlike the repeating FRB 20190520B, which also showed excess dispersion (*6*, *14*). We suggest that the excess dispersion for FRB 20220610A originates in a less magneto-ionically active plasma compared with that of FRB 20190520B, such as in the interstellar medium of the host galaxy rather than in the circumburst media hypothesized for other sources (*11*). Models of galaxy interstellar media imply that the DM of a typical spiral galaxy is unlikely to exceed a few hundred parsecs per cubic centimeter except in edge-on systems (*22*, *23*). Higher DM values can plausibly be produced by high-density clumps of gas within the host galaxy, particularly at $z \sim 1$, where galaxies have a substantially higher fraction of their baryons in gas (rather than stars) than at $z \sim 0$ (*24*). Alternatively, the dispersion could originate from structure in the foreground intergalactic medium or from additional ionized material associated with the possible galaxy merger between components (a), (b), and (c) discussed above.

Our DM analysis confirms inferences from other techniques (*25*) that the gas of the intergalactic medium is highly ionized. The detection of an FRB at $z > 1$ allows us to study the ionized plasma toward, around, and within the host galaxy. We expect a sight line to $z = 1$ to intersect the halos of several galaxies similar in mass and size to the Milky Way (*26*), which has previously been used to investigate foreground galaxy properties using FRBs (*27*).

Interpretation of the burst energy

The measured bandwidth-averaged fluence of FRB 20220610A is 45 ± 5 Jy ms (where Jy is the jansky, equal to 10^{-23} erg s^{-1} cm^{-2} Hz^{-1}), which implies an isotropic-equivalent spectral energy density of $(6.4 \pm 0.7) \times 10^{32}$ erg Hz^{-1} and a burst energy of $(6.4 \pm 0.7) \times 10^{41}$ erg (*11*). We derived the burst energy by assuming an intrinsic 1-GHz bandwidth and did not apply a redshift-dependent correction to the burst spectral energy distribution (a K-correction) (*11*). This value exceeds, by a factor of 3.5, the characteristic maximum energy E_{max} derived by previous FRB population models (*11*, *28*). It is unknown whether FRBs are emitted isotropically or only over a limited beaming angle, which would affect the inferred energetics and could vary between FRB sources (or between repeated FRBs from single sources). Assuming isotropic emission, we added FRB 20220610A to a previous sample of FRBs (*28*) and refitted the FRB burst energy distribution. We find that the best-fitting maximum energy E_{max} increases by a factor of 2.7 to $10^{41.7\,\pm\,0.2}$ erg (equivalently, the maximum energy density becomes $\log_{10}\left|\frac{E_\nu}{\text{erg Hz}^{-1}}\right| = 32.7 \pm 0.2$). In Fig. 4, we compare FRB 20220610A to the fluence of the brightest radio pulse observed from a galactic

magnetar—which is a factor of 10^5 less luminous than the burst observed from FRB 20220610A—and the wider sample of FRBs.

If a K-correction is applied, assuming a spectral index for FRB emission similar to that of the burst population found by ASKAP (*11*, *29*), we find that the burst energy integrated over the instrument bandwidth is $\sim 2 \times 10^{42}$ erg, which is higher than most localized FRBs (Fig. 4). This constrains emission models of FRBs because the electric field strength at the source can be estimated independently of the beaming angle. The calculation assumes no amplification by gravitational or plasma lensing (see supplementary text). In one class of models, FRB emission is produced near the surface of a neutron star. From the luminosity of the burst, $\sim 3 \times 10^{46}$ erg s^{-1} in the host galaxy's rest frame, we infer an electric field strength of $4.2 \times 10^{12} (r/10\ \mathrm{km})^{-1}$ V m^{-1} for a linearly polarized wave, where r (~10 km) is the curvature radius of the neutron star's magnetic field. At a neutron star surface, this value is a few percent of the Schwinger critical field strength, at which an electric field aligned parallel to the local magnetic field would be screened by electron-positron pair production (*30*). This would suppress the FRB rate above the Schwinger luminosity of $\sim 2 \times 10^{47}$ erg s^{-1} (*30*). In another class of models, FRBs are produced in a shock driven by relativistic ejecta, associated with the flare of a highly magnetized neutron star interacting with the neutron star wind. In these models, the radiative efficiency in the shock is very low ($\lesssim 10^{-5}$), and hence the required energy in the ejecta would be $\gtrsim 10^{47}$ erg, with the total flare energy being even higher. FRB 20220610A and other high-luminosity FRBs are challenging to explain in both model classes.

REFERENCES AND NOTES

1. D. R. Lorimer, M. Bailes, M. A. McLaughlin, D. J. Narkevic, F. Crawford, *Science* **318**, 777–780 (2007).
2. E. Petroff, J. W. T. Hessels, D. R. Lorimer, *Astron. Astrophys. Rev.* **30**, 2 (2022).
3. J. P. Macquart *et al*., *Nature* **581**, 391–395 (2020).
4. C. W. James *et al*., *Mon. Not. R. Astron. Soc.* **516**, 4862–4881 (2022).
5. S. Bhandari *et al*., *Mon. Not. R. Astron. Soc.* **475**, 1427–1446 (2018).
6. C. H. Niu *et al*., *Nature* **606**, 873–877 (2022).
7. R. M. Shannon *et al*., *Nature* **562**, 386–390 (2018).
8. K. W. Bannister *et al*., *Science* **365**, 565–570 (2019).
9. A. W. Hotan *et al*., *Publ. Astron. Soc. Aust.* **38**, e009 (2021).
10. C. K. Day *et al*., *Publ. Astron. Soc. Aust.* **38**, e050 (2021).
11. Materials and methods are available as supplementary materials.
12. P. A. G. Scheuer, *Nature* **218**, 920–922 (1968).
13. A. G. Mannings *et al*., Fast Radio Bursts as Probes of Magnetic Fields in Galaxies at $z < 0.5$. arXiv:2209.15113 [astro-ph.GA] (2022).
14. Y. Feng *et al*., *Science* **375**, 1266–1270 (2022).
15. D. McConnell *et al*., *Publ. Astron. Soc. Aust.* **37**, e048 (2020).
16. H. Cho *et al*., *Astrophys. J. Lett.* **891**, L38 (2020).
17. P. Kumar *et al*., *Mon. Not. R. Astron. Soc.* **512**, 3400–3413 (2022).
18. K. Aggarwal *et al*., *Astrophys. J.* **911**, 95 (2021).
19. S. Bhandari *et al*., *Astrophys. J. Lett.* **901**, L20 (2020).
20. S. Bhandari *et al*., *Astron. J.* **163**, 69 (2022).
21. Y. Guo *et al*., *Astrophys. J.* **800**, 39 (2015).
22. J. Xu, J. L. Han, *Res. Astron. Astrophys.* **15**, 1629–1638 (2015).
23. J.-F. Mo, W. Zhu, Y. Wang, L. Tang, L.-L. Feng, *Mon. Not. R. Astron. Soc.* **518**, 539–561 (2023).
24. A. Chowdhury, N. Kanekar, J. N. Chengalur, *Astrophys. J. Lett.* **941**, L6 (2022).
25. T. S. Kim *et al*., *Mon. Not. R. Astron. Soc.* **501**, 5811–5833 (2021).
26. J. X. Prochaska, Y. Zheng, *Mon. Not. R. Astron. Soc.* **485**, 648–665 (2019).
27. J. X. Prochaska *et al*., *Science* **366**, 231–234 (2019).
28. C. W. James *et al*., *Mon. Not. R. Astron. Soc.* **509**, 4775–4802 (2022).
29. J. P. Macquart *et al*., *Astrophys. J. Lett.* **872**, L19 (2019).
30. W. Lu, P. Kumar, *Mon. Not. R. Astron. Soc.* **483**, L93–L97 (2019).
31. CHIME/FRB Collaboration, *Nature* **587**, 54–58 (2020).
32. C. D. Bochenek *et al*., *Nature* **587**, 59–62 (2020).
33. P. Kumar *et al*., *Astrophys. J. Lett.* **887**, L30 (2019).
34. W. Herrmann, *The Astronomer's Telegram* **14556**, 1 (2021).
35. L. G. Spitler *et al*., *Astrophys. J.* **790**, 101 (2014).
36. J. W. T. Hessels *et al*., *Astrophys. J. Lett.* **876**, L23 (2019).
37. B. Marcote *et al*., *Nature* **577**, 190–194 (2020).
38. K. Nimmo *et al*., *Mon. Not. R. Astron. Soc.* **520**, 2281–2305 (2023).
39. V. Ravi *et al*., *Nature* **572**, 352–354 (2019).
40. R. Luo *et al*., *Nature* **586**, 693–696 (2020).
41. D. C. Price *et al*., *Mon. Not. R. Astron. Soc.* **486**, 3636–3646 (2019).
42. R. Shannon, Dataset: FRB 20220610A: Fast radio burst and host-galaxy observations, gSTAR Data Management and Collaboration Platform (2023); http://dx.doi.org/10.26185/64f7e0a9170f4.

ACKNOWLEDGMENTS

We thank K. Heintz for contributions to the FURBY project and N. Förster-Schreiber and K. Glazebrook for discussions. We thank ATNF staff for supporting the CRAFT observations with ASKAP. This work is based on observations collected at the European Southern Observatory (ESO) under programs 0105.A-0687 and 1108.A-0027. This work uses data obtained from Inyarrimanha Ilgari Bundara, the Murchison Radio-astronomy Observatory. We acknowledge the Wajarri Yamaji People as the Traditional Owners and native title holders of the observatory site. CSIRO's ASKAP radio telescope is part of the Australia Telescope National Facility (https://ror.org/05qajvd42). Operation of ASKAP is funded by the Australian government with support from the National Collaborative Research Infrastructure Strategy. ASKAP uses the resources of the Pawsey Supercomputing Research Centre. Establishment of ASKAP, Inyarrimanha Ilgari Bundara, the CSIRO Murchison Radio-astronomy Observatory, and the Pawsey Supercomputing Research Centre are initiatives of the Australian government, with support from the government of Western Australia and the Science and Industry Endowment Fund. Some of the data were obtained at the W. M. Keck Observatory, which is operated as a scientific partnership among the California Institute of Technology, the University of California, and NASA. The Observatory was made possible by the generous financial support of the W. M. Keck Foundation. We recognize and acknowledge the very important cultural role and reverence that the summit of Maunakea has always had within the indigenous Hawaiian community. We are most fortunate to have the opportunity to conduct observations from this mountain. **Funding:** S.B. is supported by a Dutch Research Council (NWO) Veni Fellowship (grant no. VI.Veni.212.058). A.T.D. and K.G. acknowledge support through Australian Research Council (ARC) Discovery Project (DP) DP200102243. A.T.D. and R.M.S. acknowledge support through ARC DP DP220102305. C.W.J. and M.G. acknowledge support through ARC DP DP210102103. R.M.S. acknowledges support through ARC Future Fellowship FT190100155. J.X.P., S.S., C.D.K., A.C.G., and N.T. acknowledge support from National Science Foundation grants AST-1911140, AST-1910471, and AST-2206490. J.X.P. is a Simons Pivot Fellow. N.T. acknowledges support through FONDECYT grant no. 11191217. **Author contributions:** S.D.R., A.C.G., L.M., N.T., J.X.P., and S.S. collected and analyzed the optical and infrared imaging and spectroscopic observations. K.W.B. developed the FRB search and localization systems with contributions from S.B. and R.M.S. A.T.D., M.G., K.G., and D.R.S. performed the FRB localization and high–time resolution processing. R.D.E. and E.M.S. provided comments on the manuscript and the interpretation of the host galaxy properties. C.W.J. and W.L. interpreted the burst energetics and implications for the FRB emission mechanism. V.A.M. developed the observatory control systems that enabled FRB searches and calibration observations. H.Q. and M.W.S. measured the burst temporal properties. S.D.R., K.W.B., A.T.D., C.W.J., and J.X.P. contributed to the drafting of the manuscript. R.M.S. led the drafting of the manuscript, coordinated the FRB searches, and measured and interpreted the burst polarimetric properties. **Competing interests:** The authors declare no competing interests. **Data and materials availability:** The raw ASKAP observations, reduced radio images and burst data, reduced optical and infrared images, and reduced optical and infrared spectra are available from the Swinburne Data Portal (*42*). The raw VLT observations are available from the ESO archive (http://archive.eso.org/eso/eso_archive_main.html) under program IDs 0105.A-0687 and 1108.A-0027.

SUPPLEMENTARY MATERIALS

science.org/doi/10.1126/science.adf2678
Materials and Methods
Supplementary Text
Figs. S1 to S8
Tables S1 and S2
References (*43*–*108*)

Submitted 12 October 2022; accepted 4 September 2023
10.1126/science.adf2678